Journal of
Synchrotron Radiation

ISSN 0909-0495

Received 10 February 2009
Accepted 2 July 2009

A first low-resolution difference Fourier map of phosphorus in a membrane protein from near-edge anomalous diffraction

Peter Boesecke,[a] Jean Marie Bois,[b] Thibaut Crépin,[b] Carola Hunte,[c]‡ Richard Kahn,[d] Wei-Chun Kao,[c]‡ Lionel Nauton,[d] Anne-Marie Lund Winther,[e] Jesper Moller,[e] Poul Nissen,[e] Hughes Nury,[d] Claus Olesen,[e] Eva Pebay-Peyroula,[d] Jean Vicat[d] and Heinrich Stuhrmann[d,f]*

[a]ESRF, F-38043 Grenoble, France, [b]EMBL, F-38043 Grenoble, France, [c]Max-Planck-Institut für Biophysik, D-60438 Frankfurt, Germany, [d]Institut de Biologie Structurale Jean-Pierre Ebel, CEA-CNRS-UJF, F-38027 Grenoble, France, [e]University of Aarhus, Department of Molecular Biology, DK-8000 Aarhus, Denmark, and [f]GKSS Forschungszentrum, D-21494 Geesthacht, Germany. E-mail: heinrich.stuhrmann@orange.fr

Crystal diffraction of three membrane proteins (cytochrome bc_1 complex, sarcoplasmic reticulum Ca^{2+} ATPase, ADP-ATP carrier) and of one nucleoprotein complex (leucyl tRNA synthetase bound to tRNAleu, leuRS:tRNAleu) was tested at wavelengths near the X-ray *K*-absorption edge of phosphorus using a new set-up for soft X-ray diffraction at the beamline ID01 of the ESRF. The best result was obtained from crystals of Ca^{2+} ATPase [adenosin-5′-(β,γ-methylene) triphosphate complex] which diffracted out to 7 Å resolution. Data were recorded at a wavelength at which the real resonant scattering factor of phosphorus reaches the extreme value of −20 electron units. The positions of the four triphosphates of the monoclinic unit cell of the ATPase have been obtained from a difference Fourier synthesis based on a limited set of anomalous diffraction data.

Keywords: anomalous dispersion; phosphorus; membrane proteins; nucleoproteins.

1. Introduction

Phosphorus is a regular constituent of a number of biomolecules found in living matter. It is relatively abundant in DNA and RNA and to a smaller extent in lipids and in some proteins. Its ubiquitous presence would make it an ideal native label for the study of the interaction of the main components of living cells. So far, there have been very few attempts in macromolecular structure research in this direction (Stuhrmann *et al.*, 1995; Biou *et al.*, 2005). All of them attempt to use the relatively strong anomalous dispersion of the atomic scattering factor of phosphorus(V), which amounts to a change of both the real and the imaginary resonant scattering factors, f' and if'', by almost 20 electron units near the X-ray *K*-absorption edge at a wavelength λ_k = 5.761 Å corresponding to a photon energy of E_k = 2152 eV (Biou *et al.*, 2005).

Interesting as this is, the use of soft X-rays in diffraction experiments means coping with a reduced penetration depth of this radiation in almost any kind of matter. The penetration depth of 5.76 Å photons in water is 20 µm, and it is 2 cm in air. These numbers impose new rules, which are rather different from those of conventional techniques of protein crystallography. The optimal set for soft X-ay diffraction is not yet at hand, but this paper will present a technical progress which has been achieved recently at the European Synchrotron Radiation Facility (ESRF).

Various types of protein crystals were tested: rod-like crystals of leuRS:tRNAleu complex, thin flat crystals of ADP-ATP carrier (Pebay-Peyroula *et al.*, 2003) and sarcoplasmic reticulum Ca^{2+} ATPase (SERCA) (Sorensen *et al.*, 2004) and the more compact crystals of the cytochrome bc_1 complex (Lange *et al.*, 2001). The choice of the samples reflects the potential of the anomalous dispersion of phosphorus for the study of the interaction of proteins with RNA and of membrane proteins with lipids.

2. Experimental

The technical design of the presently used set-up for soft X-ray diffraction has been described by Biou *et al.* (2005). Its realisation by a joint effort of the Institut de Biologie Structurale (IBS), the European Molecular Biology Laboratory (EMBL) and the ESRF is shown in Fig. 1.

‡ Present address: Institute of Membrane and Systems Biology, University of Leeds, Leeds LS2 9JT, UK.

The main part of the set-up is a cylindrical box covered by two-thirds of its jacket by a flexible image plate sensitive to (soft) X-rays. Hence, the intensity diffracted by the sample in the centre of the cylinder can be detected within the angular range −150° to +100° along the azimuth and from −52° to +66° in the orthogonal direction. With 5.76 Å X-ray photons, a wavelength close to the *K*-absorption edge of phosphorus, the largest accessible scattering angle of 150° allows for a structural resolution of 3 Å. This is one of the technical challenges in soft X-ray diffraction; another arises from the absorption of soft X-rays already mentioned above. Ideally, the beam path between the source of soft X-rays down to the detector should be completely evacuated. In practice, windows will be necessary at some places to maintain a protective atmosphere for the sample, particularly for very sensitive samples like protein crystals. Although various solutions have been suggested (Stuhrmann *et al.*, 1995; Djinović *et al.*, 2005; Biou *et al.*, 2005), the choice of a helium atmosphere appears to be convenient for two reasons: (i) helium is transparent at X-ray wavelengths below 10 Å, and (ii) cold helium gas is a good coolant of the sample. This led to the set-up shown in Fig. 1.

In most cases, helium gas cooled to 100 K by a Oxford Cryogenic System 700 is used. A major improvement with respect to the previous version (Biou *et al.*, 2005) is the double window filled with warm helium which prevents the formation of frost on the outer surface of the window. The cold helium gas leaving the central cylinder is warmed up and pumped into the double window from where it is recovered. The cryogenic system for soft X-ray diffraction has been developed by EMBL.

Table 1
Protein crystals used for soft X-ray diffraction.

Sample (PDB entry)	Phosphorus-containing molecules (no. of P atoms per molecule/[kDa])	Space group; unit cell (Å)
LeuRS:tRNAleu	tRNA (90/113)	$P2_1$; 89.0, 76.58, 90.55, β = 102.5°
Cytochrome bc_1 complex (1kb9)	Various phospholipids (6/239)	$C2$; 214.4, 163.9, 147.3, β = 117.5°
Ca^{2+} ATPase (SERCA) (1t5s)	AMPPCP‡ (3/105), various phospholipids	$C2$; 162.4, 76.3, 151.2, β = 108.7°
ADP-ATP carrier (2c3e)	Various phospholipids	$C222_1$; 76.2, 110.7, 89.5

‡ Adenosin-5′-(β,γ-methylene) triphosphate is abbreviated as AMPPCP.

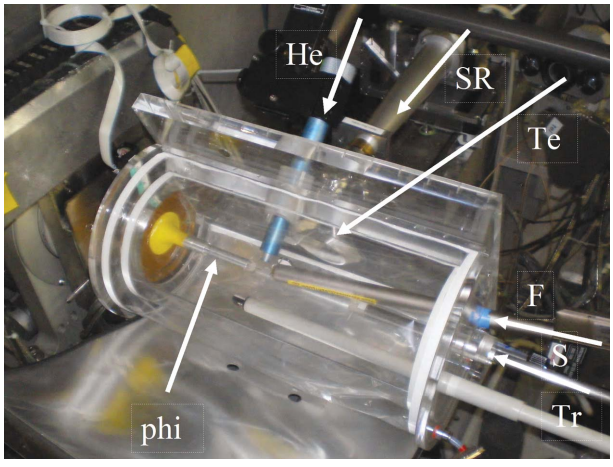

Figure 1
Set-up for soft X-ray diffraction. Monochromatic X-ray synchrotron radiation (SR) enters the cylindrical box through a beryllium window of thickness 25 µm. A jet of cold helium gas (He) cools the crystal fixed to the end of the φ-axis (phi). A telescope (Te) is used for the alignment of the crystal in the beam. The configuration shown is used for the measurement of X-ray fluorescence and the absorption by the detectors (F and Tr). These detectors will be withdrawn when the crystal is loaded using the sample transfer line (S) and when the diffracted intensity is being recorded. The cover plate of aluminium has been opened and the flexible image has been removed. Thus the above-mentioned items can be seen through the transparent double window of Mylar foils of thickness 6 µm. The radius of the bent image plate is 100 mm.

In the absence of a sample, 40% of the 5.76 Å photons arriving at the front end of the set-up shown in Fig. 1 will reach the image plate. The absorbing elements are 25 µm beryllium, 300 mm helium and 12 µm Mylar foil of the double window.

Other items of the set-up are needed for the alignment of the crystal in the X-ray beam. The special φ-axis with its long rod is one of the contributions of the ESRF to this project. The crystal is observed by a telescope in two ways, simultaneously: (i) directly and (ii) by its shadow in the soft X-ray beam on a fluorescent screen a few millimetres behind the sample. Another camera is used to align the nozzle of the helium transfer line; this explains one of the two holes in the aluminium plate (Fig. 1).

Moreover, the increase of the X-ray synchrotron radiation intensity at wavelengths near the *K*-edge of phosphorus by a factor of 10 owing to the replacement of the wiggler by a new undulator at beamline ID01 of the ESRF has been highly beneficial both to the quality of the X-ray diffraction data and to the proper functioning of a part of the optical system.

The diffracted intensity was recorded using a cylindrically bent image plate. The readout time of one picture is 10 min. With a measuring time of another 10 min, the turnaround time comes close to half an hour. The long feedback time is the only weak point of a set-up with an otherwise excellent performance.

3. Crystal diffraction at wavelengths near the *K*-absorption edge of phosphorus

The protein crystals used for diffraction experiments at wavelengths near the *K*-edge of phosphorus are listed in Table 1. The crystals were rotated by 5° in 10 min for one picture recorded by the bent image plate. All of them diffract soft X-rays. The limit of structural resolution varies strongly with the crystal used (Table 2). As the experiment was meant to test a larger number of protein crystals, data were recorded at one wavelength only for a given crystal (Table 2).

Best results were obtained from one of the SERCA crystals which showed well resolved peaks of the diffracted intensity

Table 2
Diffraction properties of the crystals; the data were recorded either at λ_1 = 5.761 Å (2152 eV) or at λ_2 = 5.755 Å (2154 eV) (see Fig. 2).

Sample	Resolution (wavelength, λ)	Remarks
LeuRS:tRNAleu	20 Å (λ_1)	Crystal mounted on polyimide grid at 269 K, frozen in helium box
Cytochrome bc_1 complex	10 Å (λ_2)	Crystal mounted on polyimide grid at 269 K, frozen in helium box
Ca^{2+} ATPase (SERCA)	7 Å (λ_1)	Frozen crystal mounted on loop, transferred to helium box
ADP-ATP carrier	20 Å‡ (λ_2)	Frozen crystal mounted on loop, transferred to helium box

‡ A better resolution has been reported by Biou *et al.* (2005).

up to 7 Å resolution at the initial scan of 5° (Fig. 3). The resolution limit varies with the orientation of the crystal; it changes to 12 Å in adjacent scan intervals and to 20 Å in more remote scan intervals. The initial scan interval was revisited twice. The diffracted intensity had decreased to half of the original value after two hours. Finally the crystal was moved to a different orientation.

The crystals of the cytochrome bc_1 complex diffract to a slightly lower resolution of about 10 Å.[1] Numerous weak diffraction peaks were observed, but mostly as streaks, between 20 Å and 10 Å resolution (Fig. 4). The indices [*hkl*] are inserted for the stronger reflections only. The crystal of the LeuRS:tRNAleu complex diffracted to 20 Å resolution (Fig. 5).

4. Difference Fourier maps of phosphorus

The spatial phosphorus density distribution $\rho_P(x,y,z)$ in a unit cell of a crystal can be obtained to a good approximation from the diffracted intensity measured at two wavelengths, *e.g.* at λ_1 and λ_2 (Fig. 2), near the *K*-absorption edge of phosphorus,

$$\rho_P(x,y,z) = (1/V)\sum_{h,k,l}\left[F_{h,k,l}(\lambda_2) - F_{h,k,l}(\lambda_1)\right] \times \exp\left(i\alpha_{h,k,l}\right)\exp[-2\pi i(hx+ky+lz)], \quad (1)$$

where $F_{h,k,l}$ is the square root of the intensity $I_{h,k,l}$. The phases $\alpha_{h,k,l}$ can be those of the known protein structure or derived by heavy-atom derivatives.

As mentioned in the previous section, diffraction data of the crystals cited in Table 2 were collected at one wavelength, λ_1 or λ_2, only (Fig. 2). Moreover, the data sets are far from being complete: around 30% at 20 Å resolution (Table 3) and even less at still higher resolution. These two facts together with the accuracy of the measured intensities of diffraction set serious limits to a difference Fourier synthesis.

In a first step, one needs to show to what extent a given set of diffracted intensities $I_{h,k,l}$ measured at a wavelength near the *K*-absorption edge agrees with the corresponding intensities calculated from the known structure. Second, one has to make sure that the agreement at the wavelength actually used is better than that obtained at other wavelengths close to the absorption edge.

Table 3
Some parameters relevant to the difference Fourier synthesis at a structural resolution of 20 Å.

n = number of measured unique reflections, *N* = number of all unique reflections. Mean values of statistical errors, ΔI, of the measured intensities of diffraction are given in columns 3 and 4. Mean values of the expected anomalous scattering intensities, I_A, based on the extreme difference in f' at the wavelengths λ_1 and λ_2 (see Fig. 2) are given in columns 5 and 6.

Protein	*n*/*N*	$\Sigma\Delta I/\Sigma I$	$(\Sigma\Delta I/I)/N$	$\Sigma I_A/\Sigma I$	$(\Sigma I_A/I)/N$
SERCA	56/153	0.028	0.059	0.050	0.144
Cytochrome bc_1	72/360	0.049	0.081	0.024	0.047
LeuRS:tRNAleu	30/105	0.050	0.128	0.207	0.310

If this is the case, the $F_{h,k,l}(\lambda)$ difference in (1) may be completed. A set of diffracted intensities obtained at short wavelengths could be a useful reference, particularly for the measurements at $\lambda = \lambda_1$, where f' is strongly negative (Fig. 2). $F_{h,k,l}(\lambda_2)$ then would be replaced by $F_{h,k,l}$ (off resonance). This approach would be less useful for the measurements at $\lambda = \lambda_2$ where the contribution of anomalous dispersion to the diffracted intensity is relatively small. This is one reason why the missing set of $F_{h,k,l}(\lambda)$ in (1) will be calculated from the model throughout. The other reason is that the large difference $f'(\lambda_2) - f'(\lambda_1) = 20$ electron units at practically no change of absorption owing to f'' provides optimal conditions for the evaluation of the phosphorus density map from a difference Fourier synthesis. As the change in wavelength on passing from λ_1 to λ_2 is very small, the trajectory of the beam through the crystal will be the same. In the absence of a systematic error which might have come from a change in absorption or a change of the beam trajectory across the

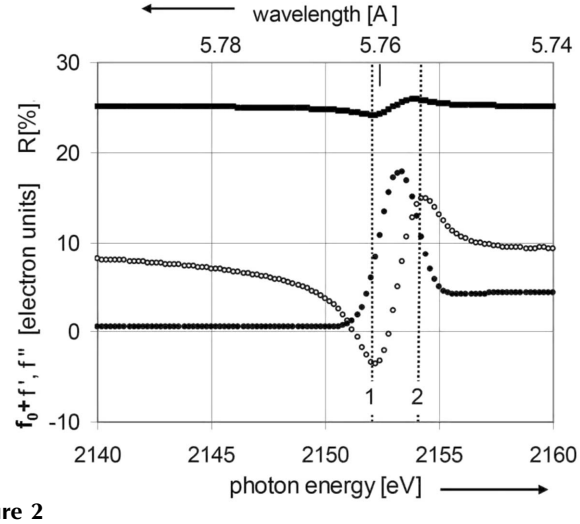

Figure 2
Anomalous dispersion of the atomic scattering factor of phosphorus, $f_0 + f'(\lambda) + if''(\lambda)$, in phospholipids (Biou *et al.* 2005), where $f'(\lambda)$ and $f''(\lambda)$ are presented by white circles and black circles, respectively. For the definition and discussion of *R* (squares), see equation (3) and §4.1, respectively.

[1] One of the crystals with a maximum size of almost 1 mm diffracted in the backwards direction. Several peaks were observed at 3.3 Å resolution, with a spacing which is not incompatible with that of the unit-cell dimensions of the cytochrome bc_1 complex.

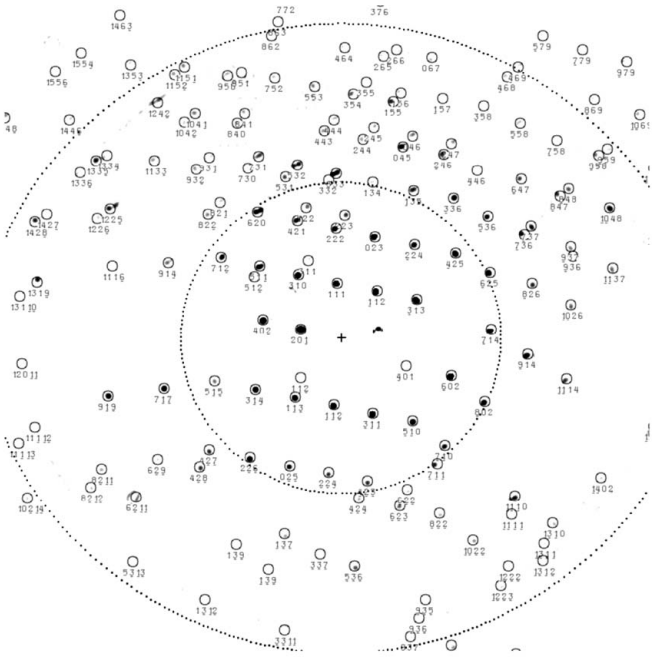

Figure 3
Diffraction of 5.762 Å photons by SERCA. The crystal was rotated by 5° in 10 min. The almost circular lines around the centre of the beam (+) delimit the 20 Å and 10 Å structural resolution. The intensity of background scattering has been removed by using a filter.

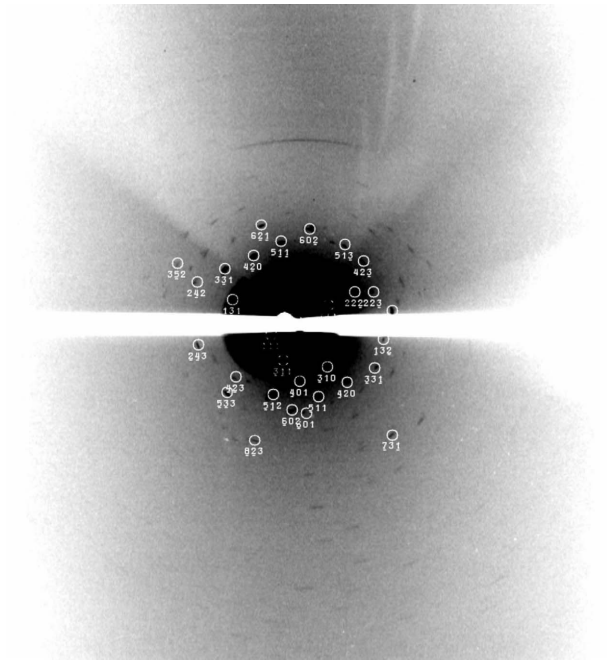

Figure 4
Diffraction of 5.755 Å photons by cytochrome bc_1. The range of structural resolution is the same as in Fig. 2. The crystal was rotated by 5° in 10 min. A constant background has been subtracted in order to enhance the visibility of the weak reflections at larger scattering angles. The white region in the middle of the picture is the shadow cast by a horizontal rod with the beam stop.

crystal, the accuracy of the intensity difference depends on the statistical error of the intensity measurements at λ_1 and λ_2 only.

Before entering into a more detailed discussion of the data, parts of which are shown in Figs. 3, 4 and 5, a summary of their statistical accuracy and of the expected intensity of anomalous diffraction within the structural resolution limit of 20 Å is presented in Table 3. Rather accurate data were obtained from SERCA crystals. Their completeness of 0.37 is slightly better than that of the data obtained from the other crystals. The triphosphates of AMPPCP are expected to give rise to a relatively strong anomalous diffraction.

The diffraction peaks from the cytochrome bc_1 complex are more numerous than with SERCA, but they are weaker. Although the ratio between the number of phosphorus atoms per protein mass is similar for SERCA and the cytochrome bc_1 complex, the expected intensity owing to anomalous dispersion of the phosphates of lipid molecules associated with the latter is considerably lower in the resolution range under discussion.

The leuRS:tRNAleu complex gives rise to a very strong contribution of anomalous scattering. The analysis is likely to be limited mainly by the low completeness of the data.

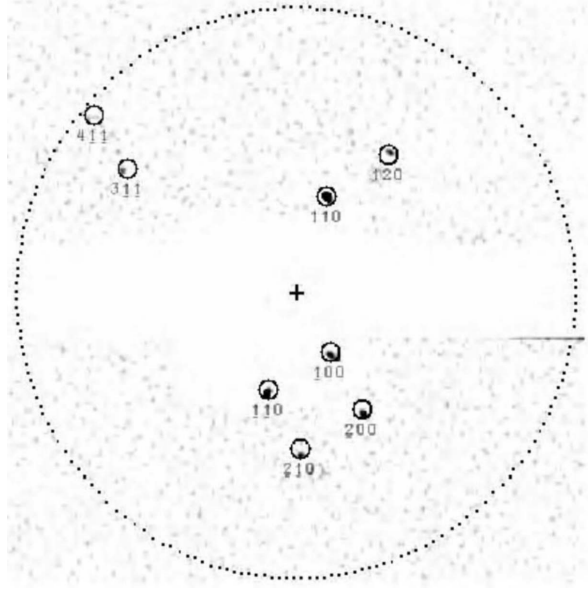

Figure 5
Diffraction of 5.762 Å photons by the leucyl tRNA synthetase tRNA complex. The crystal was rotated by 5° in 10 min. The circle around the centre of the beam (+) delimits the 20 Å structural resolution. The intensity of background scattering has been removed using a filter.

4.1. SERCA

One of the members of the family of the ATP driven cation pumps is the sarcoplasmic reticulum calcium pump from skeletal muscle (SERCA). It is a monomeric membrane protein, responsible for transporting calcium ions across biological membranes up to the limiting electrochemical gradient from the cytoplasm into sarcoplasmic reticulum (Moller *et al.*, 1996). The binding of AMPPCP to the Ca^{2+}ATPase in some sense simulates the binding of ATP (Sorensen *et al.*, 2004).

The quality of the soft X-ray diffraction patterns collected from SERCA crystals changes both with time and the orientation of the crystal with respect to the X-ray beam. Starting from the crystal orientation giving rise to the image shown in Fig. 3, the number of reflections is roughly halved in the neighbouring scan intervals, and only 10% of the reflections, mainly at low resolution, are observed in the scan intervals after next. These measurements have been repeated with the same crystal. The diffracted intensity shown in Fig. 3 decreases to half of the initial value in about two hours.

The strong variation in the quality of the diffraction pattern with the crystal orientation is somehow linked to the size and shape of the crystal and to the loop on which it is mounted. Both are more or less opaque at wavelengths near the *K*-absorption edge of phosphorus. The crystals had typical dimensions of 200 × 200 × 50 µm and rhomboid shape (Fig. 6).

The large surface of the crystal covered a major part of the loop (insert of Fig. 6). On direct incidence, 92% of the 5.76 Å photons would be absorbed by 50 µm of the protein crystal. It might well be that a larger fraction of the diffracted intensity comes from the thinner edge regions of the protein crystal.

The peak intensities obtained from the experiment were corrected for the Lorentz kinematical factor and for the polarization factor (Kahn *et al.*, 1982). A further improvement of the fit was obtained by assuming an angle-dependent probability (W) of the emission of the diffracted intensity, described by

$$W(r, \psi) = \sum_{l=0}^{L} \sum_{n=l}^{L} C_{l,n}\, r^n\, P_l(\cos\psi) \exp(-ar^2), \qquad (2)$$

where r is the distance from the centre of the diffraction pattern and ψ is the azimuth angle in the detector plane. The coefficients a and $C_{l,n}$ of the expansion as a series of Legendre polynomials, P_l, are determined by a least-squares method, where

$$R = \frac{\sum_{h,k,l} \left| I_{h,k,l}(\text{exp, corrected}) - I_{h,k,l}(\text{calc}) \right|}{\sum_{h,k,l} I_{h,k,l}(\text{calc})} \qquad (3)$$

is minimized.

W, shown in Fig. 7, takes into account various factors influencing the emission of the diffracted intensity, *e.g.* the shape of the crystal, its non-uniform opacity, radiation damage of the crystal surface which may be non-uniform, the shadow cast by the loop, and last but not least the resolution limit of the crystal.

The value of R is quite sensitive to the anomalous dispersion of phosphorus (Fig. 2). Its variation with the wavelength is similar to the dispersion of f'. R is lowest at $\lambda = \lambda_1$, *i.e.* at the wavelength which has been used for the diffraction experiment for this crystal. $F_{h,k,l}(\lambda_1)$ is now obtained as the square root of $I_{h,k,l}(\lambda_1)$. $F_{h,k,l}(\lambda_2)$ calculated from the model substitutes for the missing experimental data $I_{h,k,l}(\lambda_2)$.

At 20 Å resolution, all the phosphorus atoms of a triphosphate contribute jointly to the anomalous diffraction with a weight which is comparable with that of a heavy atom. A

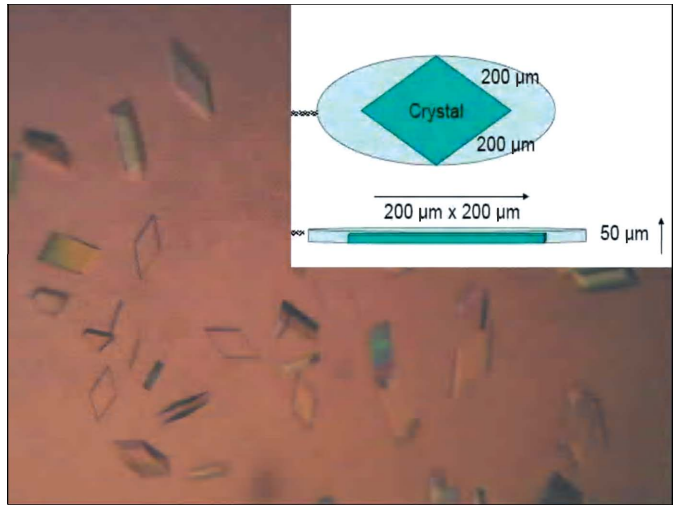

Figure 6
Crystals of the calcium and nucleotide bound form, Ca2E1:AMPPCP, of SERCA. Insert: the crystal mounted on a loop.

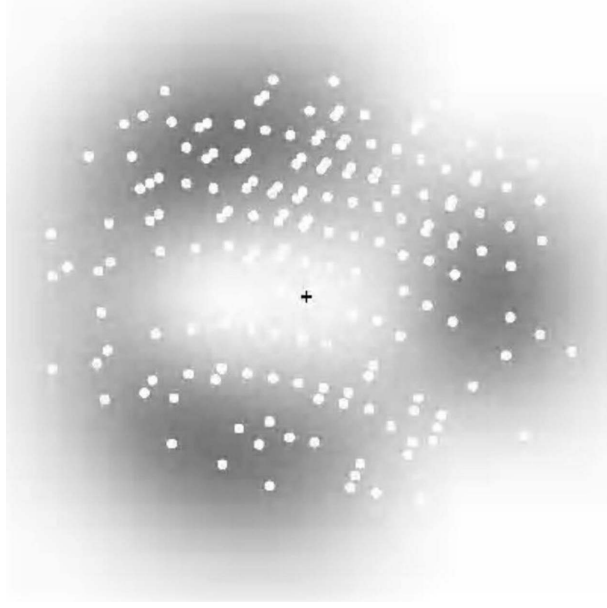

Figure 7
The probability $W(r, \psi)$ of the emission of 5.76 Å photons diffracted by a crystal of SERCA. The series (2) has been terminated at $L = 4$. The diffraction pattern is that shown in Fig. 3.

difference Fourier synthesis starting from $F_{h,k,l}(\lambda_1)$ and $F_{h,k,l}(\lambda_2)$ at 20 Å resolution calculated from the known structure (Sorensen *et al.*, 2004) shows the sites of the triphosphates of the SERCA–AMPPCP complex as intense spots (Fig. 8).

The result of the difference Fourier synthesis starting from a mixture of experimental and calculated $F_{h,k,l}$ is shown in Fig. 9. The phosphorus density map clearly shows the sites of the phosphorus atoms of AMPPCP as large intense spots, that are elongated mainly due to the low completeness of the data.

4.2. Cytochrome bc_1 complex

Tightly bound phospholipids are essential for the activity of the cytochrome bc_1 complex, an integral membrane protein of

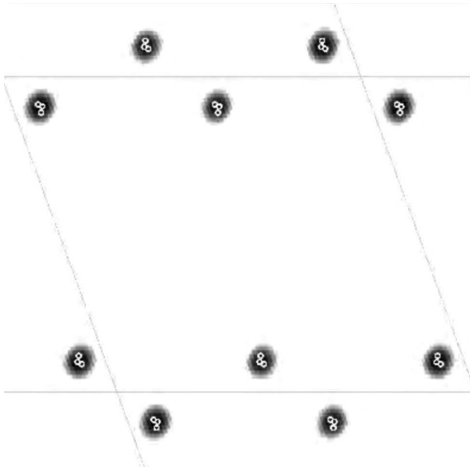

Figure 8
Difference Fourier map (grey spots) obtained from the model of SERCA at 20 Å resolution showing the sites of the phosphorus atoms (circles) of adenosine 5′-(β,γ-methylene) triphosphate as a projection onto the *ac* plane of the monoclinic unit cell of SERCA. Half the maximum peak height is reached at the edge of the grey spots. The picture covers 220 Å × 220 Å.

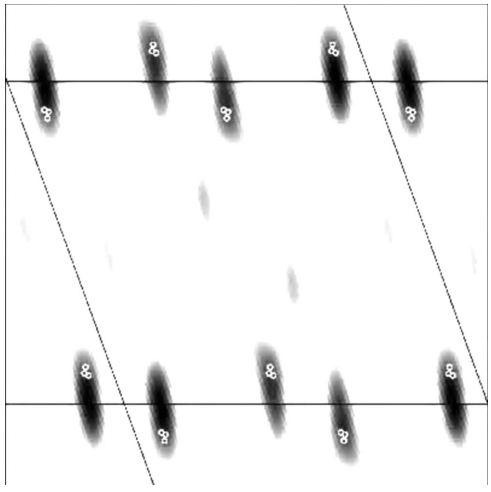

Figure 9
Difference Fourier map (grey spots) as obtained from experimental data showing the sites of the phosphorus atoms (circles, superimposed from the analysis performed in Fig. 8) of adenosine 5′-(β,γ-methylene) triphosphate as a projection onto the *ac* plane of the monoclinic unit cell of SERCA. Half the maximum peak height is reached at the edge of the grey spots.

the respiratory chain (Lange *et al.*, 2001). There are two phosphatidylethanolamines (PEs), one phosphatidylcholin (PC), one phosphatidylinositol (PI), and one cardiolipin (CL) bound to the cytochrome bc_1 complex. A difference Fourier synthesis starting from $F_{h,k,l}(\lambda_1)$ and $F_{h,k,l}(\lambda_2)$ at 20 Å resolution calculated from the known structure reveals the sites of the phosphorus atoms. The two phosphorus atoms of cardiolipin at 7 Å distance give rise to a single spot (CL in Fig. 10) in the phosphorus density map. The projection of the map along the *b*-axis is shown in Fig. 10. This result is expected from a complete set of data measured at two wavelengths λ_1 and λ_2 near the *K*-absorption edge of phosphorus.

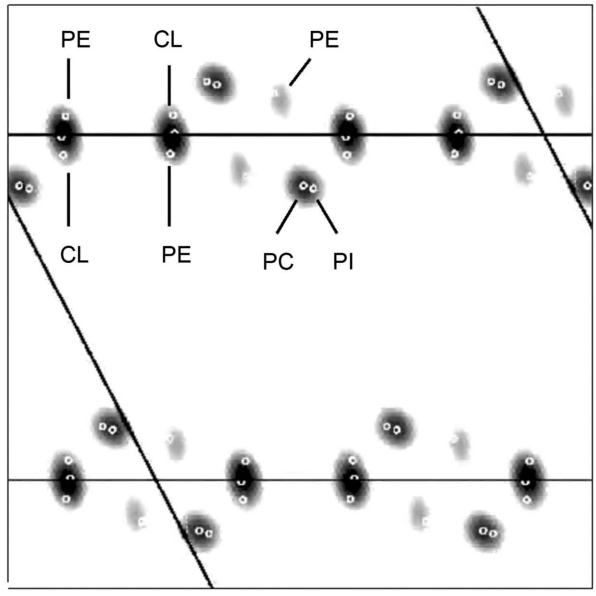

Figure 10
Difference Fourier map (grey spots) obtained from the model of the cytochrome bc_1 complex at 20 Å resolution showing the sites of the phosphorus atoms (circles) as a projection onto the *ac* plane of the monoclinic unit cell of the cytochrome bc_1 complex. Half the maximum peak height is reached at the edge of the grey spots. The picture covers 220 Å × 220 Å.

The diffraction experiment was carried out at the wavelength λ_2 (Fig. 2). The difference Fourier synthesis starts from a mixture of experimental $F_{h,k,l}(\lambda_2)$ and $F_{h,k,l}(\lambda_1)$ calculated from the model. The statistical accuracy of the experimental data, their completeness and the expected intensity of anomalous diffraction at 20 Å resolution are all lower than in the preceding case of SERCA (Table 3). Hence, the variation of R (not shown here) with the wavelength is much less pronounced than with SERCA (Fig. 2): $R(\lambda_2) - R(\lambda_1) = -0.015$. The positions of only three of the six phosphorus atoms appear to be reasonably well resolved along the *a*-axis and hardly at all along the *c*-axis (Fig. 11).

4.3. LeuRS:tRNAleu complex

The leucyl-tRNA synthetase is an enzyme that catalyzes the esterification of leucine to its cognate tRNAleu. The intermediate LeuRS:tRNAleu complex is an example of a nucleic acid protein interaction. As such it is rich in phosphorus. The expected intensity of anomalous diffraction at 20 Å resolution is large (Table 3). The phosphorus density map from a difference Fourier synthesis using $F_{h,k,l}(\lambda_1)$ and $F_{h,k,l}(\lambda_2)$ from the known crystal structure as determined by one of us (TC) is shown in Fig. 12. This result would have been obtained from a complete set of data measured at two wavelengths λ_1 and λ_2 near the *K*-absorption edge of phosphorus (Fig. 2).

The diffraction experiments were carried out at the wavelength λ_1. The change in the diffracted intensity owing to the dispersion of phosphorus is much more important than the statistical error. The spatial distribution of the phosphorus

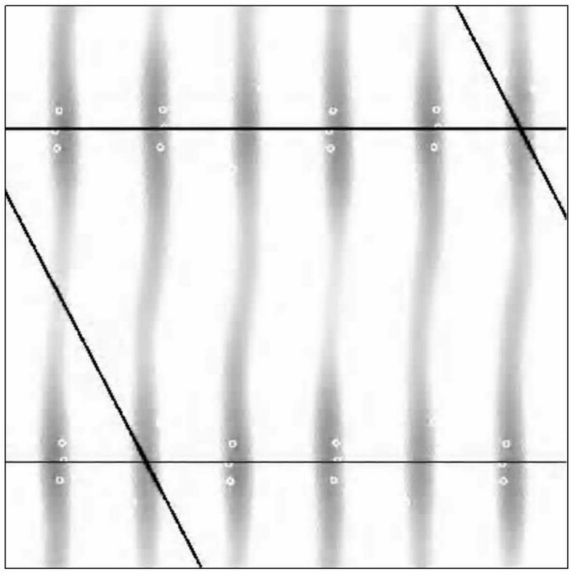

Figure 11
Difference Fourier map (grey spots) as obtained from experimental data showing the sites of the phosphorus atoms (circles, superimposed from the analysis performed in Fig. 10) as a projection onto the *ac* plane of the monoclinic unit cell of the cytochrome bc_1 complex. Half the maximum peak height is reached at the edge of the grey spots.

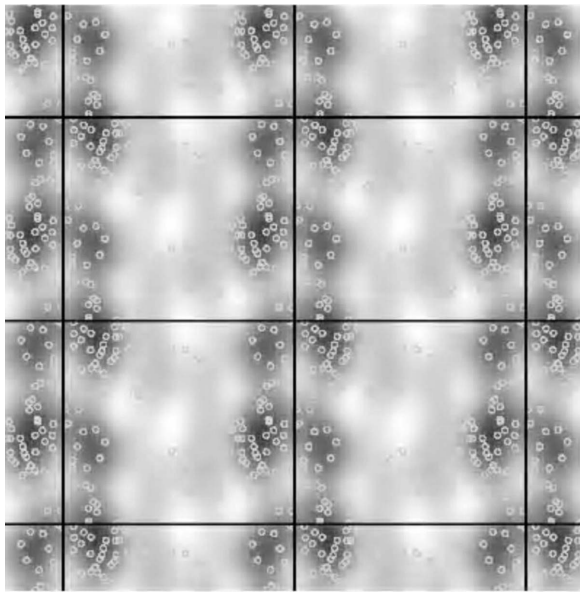

Figure 12
Difference Fourier map (grey spots) obtained from $F_{h,k,l}(\lambda_2) - F_{h,k,l}(\lambda_1)$ calculated from the model of the leuRS:tRNAleu complex at 20 Å resolution showing the sites of the phosphorus atoms (circles) as a projection onto the *ab* plane of the monoclinic unit cell of the leuRS:tRNAleu complex. The picture covers 220 Å × 220 Å.

atoms of tRNA obtained by the difference Fourier synthesis using the experimental data is best resolved in the projection onto the *ab* plane (Fig. 13). It agrees fairly well with the corresponding difference Fourier synthesis at 20 Å resolution starting from the known structure of the leuRS:tRNAleu complex shown in Fig. 12.

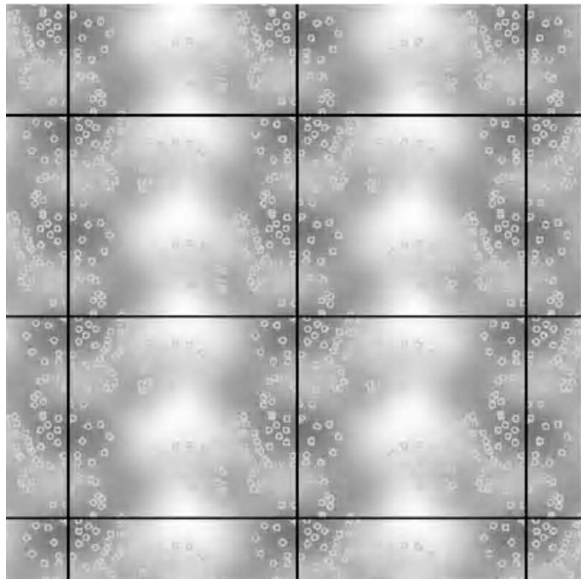

Figure 13
Difference Fourier map (grey spots) as obtained from experimental data showing the sites of the phosphorus atoms (circles, superimposed from the analysis performed in Fig. 12) of tRNA as a projection onto the *ab* plane of the monoclinic unit cell of the leuRS:tRNAleu complex.

5. Outlook

From the results shown in Figs. 9, 11 and 13, it appears that there is plenty of room for further improvement of the measurement of anomalous diffraction from protein crystals near the *K*-absorption edge of phosphorus. The gain in structural information from a phosphorus density map as obtained from a difference Fourier synthesis using complete data sets taken at λ_1 and λ_2 would be considerable, even at a structural resolution of 20 Å, as shown in Figs. 8, 10 and 12. The head groups of phospholipids interacting with membrane proteins or taking part in lipid bilayer arrangements in type 1 membrane protein crystals (Deisenhofer & Michel, 1989) could then be localized providing for a deeper understanding of protein–membrane interactions. Furthermore, the contours of nucleic acids bound to proteins could be visualized. Needless to say that close arrangements of phosphorus atoms as they occur in cardiolipin or in triphosphates are most easily detected.

Another lesson to be learned from our experiment is that the quality of the diffraction pattern may vary strongly with the orientation of the crystal with respect to the X-ray beam. A more detailed study of this behaviour might help to optimize the conditions of soft X-ray diffraction.

There is also a loss of the intensity diffracted by a protein crystal after prolonged irradiation with soft X-rays. At a temperature of 100 K, the intensity decreases to half of the initial value within two hours. Earlier experiments at a wavelength near the M_V edge of uranium (λ_{MV} = 3.5 Å) showed that there was hardly any degradation of a lysozyme crystal within a period of 12 h at a temperature of 40 K maintained by cold helium gas (Chesne, 2002). Whether this is a general property of soft X-ray diffraction at lower temperatures needs to be shown.

As protein crystals may suffer from radiation damage, it is important to measure the intensity of diffraction at two wavelengths at the absorption edge (*e.g.* at λ_1 and λ_2 mentioned above) almost simultaneously. Using an image plate as a detector, this can be achieved by recording the intensity diffracted by the crystal at λ_1 and λ_2 on one image where the corresponding two sets of diffraction peaks have been separated by a small shift of the plate (Chesne, 2002).

Image plates are very convenient detectors for soft X-ray diffraction. Being flexible, they can cover a large solid angle of X-ray diffraction as shown in Fig. 1. Data taking could be a lot faster with an on-line readout system for flexible image plates. The better solution appears to be a new type of detector, a semiconductor pixel array, PILATUS, which has been developed at the Paul Scherrer Institut (PSI), Villigen. It combines a large solid angle, fast readout and a sensitivity for soft X-rays at 2.1 keV which can be high (Bitter *et al.*, 2006).

The soft X-ray diffraction experiments reported in this paper are a part of the project MX518, to which beam time at ID01 of the ESRF had been allocated. Important contributions to the project came from the Institut de Biologie Structurale Jean-Pierre Ebel (IBS), the European Molecular Biology Laboratory (EMBL) and the European Synchrotron radiation Facility (ESRF). The support by Otto Dideberg (IBS) and Stephen Cusack (EMBL) is gratefully acknowledged.

References

Biou, V., Bösecke, P., Bois, J.-M., Brandolin, G., Kahn, R., Mas, C., Nauton, L., Nury, H., Pebay-Peyroula, E., Vicat, J. & Stuhrmann, H. (2005). *J. Synchrotron Rad.* **12**, 402–409.

Bitter, M. L., Broennimann, Ch., Eickenberry, E. F., Hill, K. W., Ince-Cushman, A., Lee, S. G., Rice, J. E. & Scott, S. (2006). *IEEE Nucl. Sci. Symp. Conf. Record*, R06-37, pp. 3721–3723.

Chesne, M. L. (2002). Thesis. Université Joseph Fourier, Grenoble, France.

Deisenhofer, J. & Michel, H. (1989). *EMBO J.* **8**, 2149–2170.

Djinović Carugo, K., Helliwell, J. R., Stuhrmann, H. & Weiss, M. S. (2005). *J. Synchrotron Rad.* **12**, 410–419.

Kahn, R., Fourme, R., Gadet, A., Janin, J., Dumas, C. & André, D. (1982). *J. Appl. Cryst.* **15**, 330–337.

Lange, C., Nett, J. H., Trumpower, B. L. & Hunte, C. (2001). *EMBO J.* **20**, 6591–6600.

Moller, J. V., Juul, B. & le Maire, M. (1996). *Biochim. Biophys. Acta*, **1286**, 1–51.

Pebay-Peyroula, E., Dahout-Gonzales, C., Kahn, R., Trézéguet, V., Lauqin, G. J.-M. & Brandolin, G. (2003). *Nature (London)*, **426**, 39–44.

Sorensen, T. L., Moller, J. V. & Nissen, P. (2004). *Science*, **304**, 1672–1675.

Stuhrmann, S., Hütsch, M., Trame, C., Thomas, J. & Stuhrmann, H. B. (1995). *J. Synchrotron Rad.* **2**, 83–86.